Research in Astron. Astrophys. Vol.0 (200x) No.0, 000–000
http://www.raa-journal.org *http://www.iop.org/journals/raa*

***R**esearch in*
***A**stronomy and*
***A**strophysics*

. . . . . .

Key words: – radiation mechanisms: thermal – ISM:atoms – ISM:HII regions – ISM:molecules

arXiv:1304.5354v1 [astro-ph.GA] 19 Apr 2013

Properties of the UCHII region G25.4NW and its associated molecular cloud

M. Ai[1], M. Zhu[1] and L. Xiao[1]

National Astronomical Observatories, Chinese Academy of Sciences, 20A, Datun Road, Chaoyang District, Beijing 100012, China

Abstract UCHII G25.4NW is a bright IR source in the inner Galaxy region. New HI images from the VLA Galactic Plane Survey (VGPS) show clear absorption features associated with the UCHII region up to 95 km s^{-1}, and there is not any other absorptions up to the tangential velocity. It reveals that G25.4NW is at a near-side distance of 5.7 kpc, and it is located in the inner Galactic molecular ring region. Using the new distance, the bolometric luminosity of G25.4NW is estimated as $10^{5.6}$ $L_{\odot}$, which corresponds to an O6 star. It contains 460 $M_{\odot}$ of ionized gas. High-resolution ^{13}CO image from the Galactic Ring Survey (GRS) reveals that G25.4NW is part of a more extended star-formation complex with about 10^4 $M_{\odot}$ molecular gas.

1 INTRODUCTION

Massive star formation play an important role in galaxy evolution. Ultra compact HII (UCHII) regions are indicators of high mass star formation sites. In these regions, newly born stars are still embedded in their natal molecular clouds. The energy from the central massive stars are absorbed by the ambient dust and reradiated in the infrared (IR), making UCHII regions among the brightest IR sources in the Galaxy.

G25.4NW is an UCHII region first identified by Lester et al. (1985), which is found to have the highest FIR luminosity in the inner spiral arm region, hosted in a giant molecular cloud (GMC) G25.4−0.14. It is also on the top two list of IR-luminosity among the 18 radio-selected UCHII regions studied by Giveon et al. (2007). Recently, a massive protostar (6-12 $M_{\odot}$) is found in a massive SCUBA core JCMT18354-0649S (Zhu et al. 2011), which is about 1′ south of G25.4NW. It is believed to lie in the same molecular cloud as G25.4NW based on the smooth change of ^{13}CO and ^{18}CO spectral profiles. Spectral line studies of JCMT18354-0649S show that both infall and outflow motions are seen in the envelope gas that surrounds this source (Wu et al. 2005; Liu et al. 2011; Carolan et al. 2009), suggesting that this source is actively accumulating material and thus can potentially grow to a even more massive object as it evolves. It's a middle mass object, and might be in a early state as a precursor of the UCHII region. Hence the G25.4NW and JCMT18354-0649S region is one of the most active star forming sites in the inner spiral arm region.

However, there was considerable uncertainty about the distance to the UCHII region G25.4NW. Downes et al. (1980) and Turner (1979) assigned a far side distance to G25.4NW based on absorption features in the H_2CO and OH lines at 96 km/s, which was thought to be close to the tangent point

⋆ E-mail: aimei,mz,xl@nao.cas.cn

velocity. Solomon et al. (1987) suggested a far-side distance of 11.5 kpc, based on the scale height of molecular cloud. The papers of Lester et al. (1985); Churchwell et al. (1990) used the far-side distance of 9.8 kpc for the UCHII region G25.4NW and they estimated a far-IR luminosity of $L_{\rm FIR} = 10^{6.238}$ $L_\odot$, indicating the presence of an O4 or O5 star. However, Giveon et al. (2007) found that the mid-IR spectral type of G25.4NW was consistent with a B1 or an O9-O7 star (based on the mid-IR dust temperature, with a $L_{\rm MIR} = 10^{4.3} - 10^{5.2}$). This suggests that the stars are not as hot as indicated by the far-IR data.

In the case of JCMT18354-0649S, Zhu et al. (2011) also found that if the far-side distance of 9.6 kpc was used, the mass of the central protostar derived from SED modeling would be as high as 10-20 $M_\odot$, and the temperature would be 4000-10,000 K, equivalent to a B2 star or earlier. Such a star should have detectable radio continuum and strong 24 μm MIR emission, which is in contradiction with observational evidences. On the other hand, the near-side distance of 5.7 kpc results in more reasonable physical parameters for JCMT18354-0649S.

Early exploration have mixed the emission and absorption spectra of G25.4NW with the nearby giant HII region W42 (Blum et al. 2000) towards this direction due to low resolution. And the methods of using the OH absorption feature and scale height method carry a large uncertainty. Anderson & Bania (2009) has used the HI Emission/Absorption method with high resolution VGPS and SGPS HI survey data to resolve the kinematic distance ambiguity for a inner Galaxy HII regions sample. In the catalogue, they quoted a near-side distance of 5.9 kpc for G25.4NW. In this paper, we present the HI absorption feature associated with the UCHII region G25.4NW to confirm the near-side distance result, and give new estimates to the related physical parameters, such as the FIR luminosity and spectral type of the massive stars in G25.4NW. Using GRS ^{13}CO (1–0) data, we also discuss the molecular cloud environment of the UCHII region.

2 DATA

The radio continuum at 1420 MHz and HI emission data sets were obtained from the Very Large Array (VLA) Galactic Plane Survey (VGPS), described in details in Stil et al. (2006). The continuum images of G25.4NW shown in this paper have a spatial resolution of 1′ at 1420 MHz and an rms sensitivity of 0.3 K ($T_b/S_\nu = 168$ K Jy^{-1}). The synthesized beam for the HI line images is also 1′, the radial velocity resolution is 1.56 km s^{-1}. The short-spacing information for the HI spectral line images comes from additional observations performed with the 100 m Green Bank Telescope of the NRAO.

The ^{13}CO-line(J=1−0) data sets are from the Galactic ring survey (Jackson et al. 2006) carried out with the Five college Radio Astronomy Observatory 14 m telescope. The CO-line data used in this paper have a velocity coverage of −5 to 135 km s^{-1}, an angular resolution of 45″ with 22″ sampling, a radial velocity resolution of 0.21 km s^{-1}, and an rms noise of $\sim$ 0.13 K.

The Spitzer 8.0μm images are taken from the Galactic Legacy Infrared Mid-Plane Survey Extraordinaire (GLIMPSE; Benjamin et al. (2003)) using the Infrared Array Camera (IRAC) (Fazio et al. 2004). The IRAC data were processed by the GLIMPSE team; image mosaics were created using the GLIMPSE pipeline after artifacts such as cosmic ray, stray light, column pull-down, and banding had been removed.

3 RESULTS AND ANALYSIS

3.1 Continuum images

Fig. 1(left) shows the VGPS 1420 MHz continuum contours overlaid on the ^{13}CO integrated intensity image (over the range 90-101 km s^{-1}) for the G25.4-0.14 region. Two radio sources, separated by about 2′, are marked in the map, namely G25.4NW (l=25.40°, b=-0.14°)at and W42 (l=25.38°, b=-0.18°). The later is also named as G25.4SE in Lester et al. (1985). A massive protostar JCMT18354-0649IRS1a was recently discovered at about 1′ south of G25.4NW (Zhu et al. 2011), which is marked as a plus sign. Contours of the 1420 MHz continuum emission starting from 67 K in steps of 57 K define a roughly circular region with a diameter of $\sim$ 1.2′. As shown in Lester et al. 1985, G25.4NW has a size of about 25″ which is not resolved in this map.

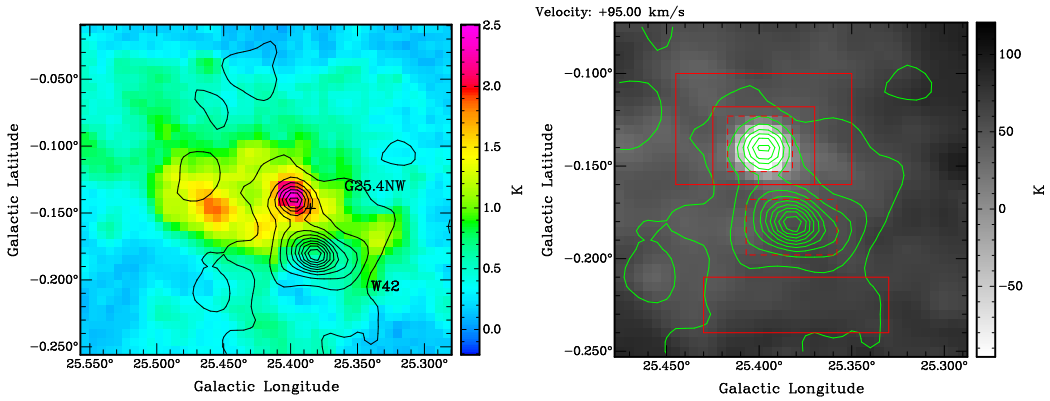

Fig. 1 The VGPS 1420 MHz continuum contours of G25.4NW overlaid on (left) the ^{13}CO integrated intensity image (over the range 90-101 km s^{-1}) and HI single-channel map (right) at 95 km s^{-1} for the GMC G25.4-0.14 region. Contours of the 1420 MHz continuum emission of the 3×σ (σ = 1 K) level above the background emission of 29 K, and then starting from 67 K in steps of 57 K are overlaid on it. The plus sign marks the position of the massive protostar JCMT18354-0649IRS1a found by Zhu et al. (2011).

3.2 The HI absorption spectra and kinematic distance

We have searched the VGPS data with the radial velocity ranging from −113 to 165 km s^{-1} for features in HI absorption which might be related to the morphology of G25.4NW. There are HI absorption features towards the direction of the HII region at the following velocity: 5, 20, 40, 50, 55, 67, 95 km s^{-1}. These HI absorption features towards the continuum intensity of G25.4NW are caused by absorption in HI clouds between the HII region and the earth. Figure 1 (right) shows the map of HI absorption at the channel of the highest absorption velocity of 95 km s^{-1}. The map has superimposed contours of 1420 MHz continuum emission which mark the HII regions.

We construct the HI emission and absorption spectra of G25.4NW in the same way as developed by Tian & Leahy (2008); Anderson & Bania (2009). To minimize the potential difference in the HI distribution along the two lines of sight (on-source and background), a background region is chosen near the continuum peak, as shown in Fig. 1 (right). Assuming that the spin temperature and optical depth of the background region are similar to that of the on-source region, the resulting difference in brightness temperature at velocity v is given by: $\Delta T(v) = T_{\rm off}(v) - T_{\rm on}(v) = T_{\rm c}(1 - e^{-\tau(v)})$. Here $T_{\rm on}(v)$ and $T_{\rm off}(v)$ are the average HI brightness temperatures of the HII region and the adjacent background region from a selected area. $T_{\rm c}$ is the average continuum brightness temperatures of the HII region. $\tau(v)$ is the HI optical depth from the continuum source to the observer.

Figure 2 (upper left panel) shows the source and background HI emission and the absorption spectra for the selected region on top of G25.4NW. The $T_{\rm on}$ is obtained by averaging over the region outlined by a dash-line box (Fig 1 right). The respective off-source region is defined by the region between two solid-line boxes, within which the $T_{\rm off}$ is obtained. The averaged continuum temperature of G25.4NW is 154 K. Figure 2 clearly reveals strong absorption features at 5, 20, 40, 50, 55, 67, 95 km s^{-1}. The highest absorption velocity detected is close to the tangential velocity of 120 km s^{-1}, but there is not

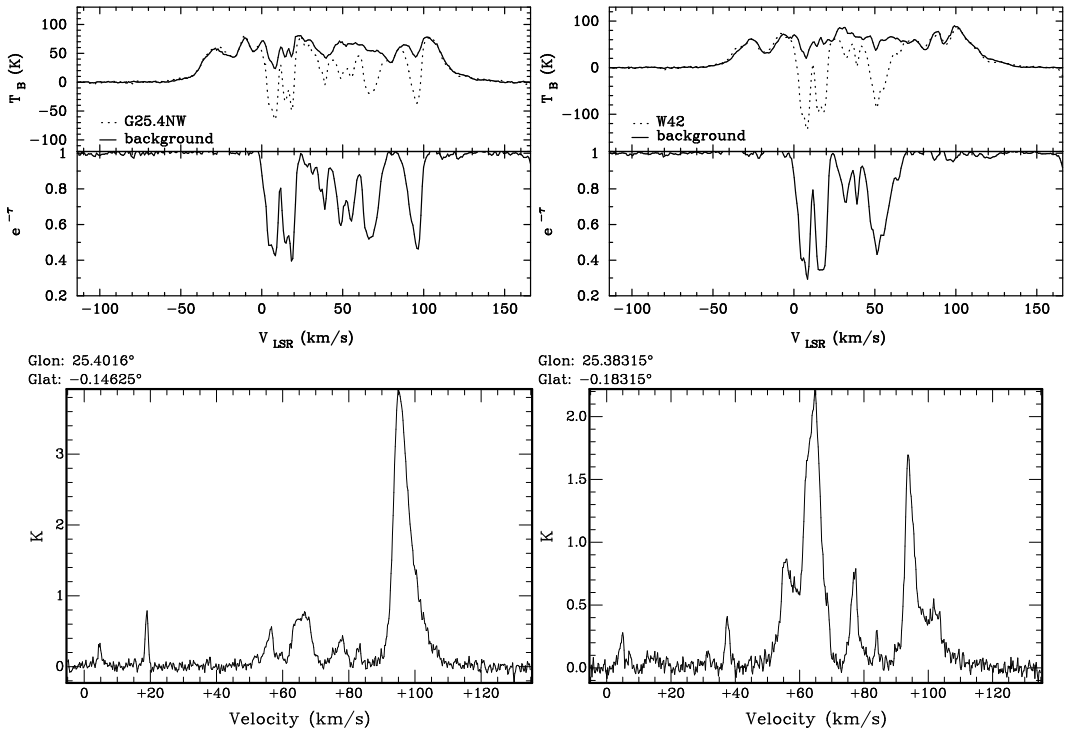

Fig. 2 Upper panels: HI emission and absorption spectra extracted from the boxes around G25.4NW (left) and W42 (right) indicated in Fig. 1. Lower panels: Averaged ^{13}CO emission spectra of the G25.4NW (left) and W42 (right) region. The 90-101 km s^{-1}emission peak in W42 ^{13}CO spectra comes from the G25.4NW molecular cloud due to the box selection.

any absorption feature between them, which indicates a near-side distance. Taking a circular Galactic rotation curve model, and using the latest estimates of the model parameters, i.e. V_0=220 km s^{-1}and R_0=8.5 kpc (Fich et al. 1989), we can determine the kinemtic distance using the distance-velocity curve as illustrated in Figure 3. The highest absorption velocity feature at 95 km s^{-1} corresponds to a near-side distance of 5.7 kpc.

For comparison, we also produce the HI absorption spectrum for the selected region of W42, as shown in the upper right panel of Figure 2. The averaged continuum temperature of W42 is 225 K. The highest HI absorption feature lies at 50−65 km s^{-1}. It is far away from the tangential velocity of 120 km s^{-1}, indicates also a near-side distance of 4.6 kpc. The 90-101 km s^{-1}emission peak in W42 ^{13}CO spectra comes from the G25.4NW molecular cloud due to the box selection, and high resolution observation will solve this problem.

The optically thin ^{13}CO emission could clearly reveal the distribution of molecular clouds along the direction of the HII region, and will indicate possible origin of these HI absorption features. Figure 2 (lower left panel) shows an average ^{13}CO spectrum for the full velocity range in the direction of G25.4NW. It shows 7 molecular components with high brightness temperature, at radial velocities of 5, 18, 55, 65, 78, 83, 95 km s^{-1} respectively. Most of the ^{13}CO emission peaks appear to be associated with an HI absorption feature, and the ^{13}CO emission velocities are consistent with the spiral arm radial velocities of the Milky Way based on the Galactic arms scheme (Cordes & Lazio 2002). In Table 1 we list the respective spiral arm radial velocities and possible associations with ^{13}CO emission or HI absorption features. Cases are included even when the velocities are up to ∼10 km s^{-1} different, since the

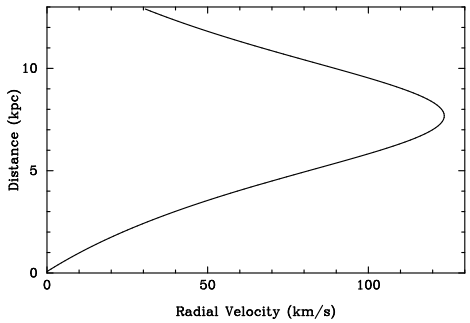

Fig. 3 The relation between the distance and radial velocity for the assumed rotation curve.

Table 1 Summary of HI and CO velocity features

Crossing number	local	1	2	3	4	5	6
Central velocities of the model spiral arms (km s^{-1})	0	26	71	93	52	21	0
G25.4NW HI absorption feature	0-10	10-20	60-80	90-100			
G25.4NW CO emission feature	5	15-20	75-85	90-100	50-60	15-20	5
W42 HI absorption feature	0-10	15-20	50-65				
W42 CO emission feature	5	32	60-70	90-100	50-60	15-20	5

calculated arm crossing velocities are based on a circular rotation model and can be off by ∼10 km s^{-1} due to non-circular motions from spiral arm shocks and velocity dispersion.

In summary, both W42 and G25.40-0.14 are at the near side distance, and they appear to be located in the inner galactic CO ring at 4-6 kpc.

4 DISCUSSION

4.1 Infrared emission

Dust associated with HII regions can absorb radiation from the exciting stars of the nebulae and re-emit in the infrared wavelengths. If there is sufficient spatial coverage and optical depth of dust surrounding an HII region, measurement of the infrared flux from the HII region can provide information on the bolometric luminosity (L_{bol}) of the exciting stars.

We collect the total MIR flux densities of the IR counterparts for G24.5NW in the literature, including data from the *MSX* point-source catalog (8.3, 12.1, 14.7, and 21.3 μm), Keck I 10 m telescope (11.7, 17.65, 24.5 μm) (Giveon et al. 2007), IRAS 100 μm (Lester et al. 1985), CSO (350 μm) and SCUBA (450 μm, 850 μm) (Wu et al. 2005). *MSX* had a beam of 18.3″, and the KecK's data had an aperture of 10.5″. The 100 μm's beam is 50″, which is much larger than that of the CSO and SCUBA data. We used an aperture of 50″ to derive the sub-millimeter fluxes in order to cover the whole HII region. The dust emissivity index (β) has been estimated to be a typical value of 2.0 (Zhu et al. 2011). Thus we used a modified single temperature blackbody curve, $\nu^2 B_\nu(T_d)$ to fit the data and derive the spectral engergy distribution (SED). In lieu of a radiative transfer model, we have chosen to fit the cold component of the emission (100−850 μm) because it contains the bulk of the source luminosity. The SED fitting is plotted in Fig. 4. The best fit parameter is T_d=42.5±3 K. It is larger than that estimated in Zhu et al. (2011), considering the contribution of MIR data in the SED fitting, which trace the central bright temperature component.

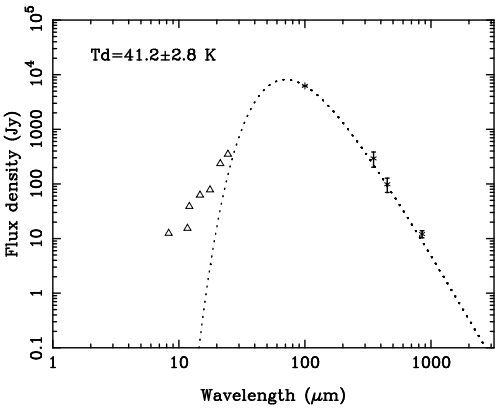

Fig. 4 Flux density distribution of G25.4NW fitted with a one-component modified blackbody model. The line marks the best fit to the 100, 350, 450, 850μm flux densities.

Table 2 Summary of observed flux densities of G25.4NW

Wavelength (μm)	Flux (Jy)	error (Jy)	aperture ($''$)
8.3	12.51	–	18.3
12.1	38.86	–	18.3
14.7	62.48	–	18.3
21.3	235.88	–	18.3
11.7	15.4	0.5	10.8
17.7	78.0	3	10.8
24.5	350.0	80	10.8
100	6240.0	–	50
350	293.0	91	50
450	98.7	29	50
850	12.1	1.8	50

For a distance of 5.7 kpc we obtain $\log(L_{bol}/L_{\odot})$=5.6. This value is lower than the result of Churchwell et al. (1990) which was estimated from the far-IR data using a far-side distance. Thus the central stars are not as hot as estimated before, and an O6 star is expected for such bolometric luminosity. (Panagia 1973).

4.2 Radio emission

Radio continuum measurements of HII regions can provide a lower limit to the total number of ionizing photons (N_L) and estimates of the average excitation parameter (U). Assuming an optically thin, spherical, constant-density HII region, the equations used are as follows (Rudolph et al. 1996),

$$N_L = 7.5 \times 10^{43} S_\nu d^2 \nu^{0.1} T_e^{-0.45} \ [\mathrm{s}^{-1}] \quad (1)$$

$$U = 1.33 S_\nu^{1/3} d^{2/3} \nu^{1/30} T_e^{0.116} \ [\mathrm{pc\ cm}^{-2}] \quad (2)$$

where ν is the frequency in GHz, S_ν is the flux density measured at frequency ν in mJy, d is the distance to the source in kpc, and T_e is the electron temperature in units of 10^4 K. Parameter values used are

ν=1.42 GHz, d = 5.7 kpc, and T_e = 10000 K. A general value of 10^4 K is used because the results of both N_L and U are not sensitive to T_e,

The flux density for G25.4NW obtained from the VGPS continuum image is 1.35 ± 0.2 Jy, which is in agreement with Giveon et al. (2007) from an VLA B configuration 1.4 GHz survey with a resolution of $\sim 5''$. This yields a value of $N_L = (3.4 \pm 0.2) \times 10^{48}$ s^{-1}, $U = 47.5 \pm 10$ pc cm^{-2}. Comparing these values (logN_L=48.5) to that of Panagia (1973), we estimate an ionizing flux and excitation parameters corresponding to an O6−O7 class star. From the 3-color HKL′ band image (Fig. 3 in Zhu et al. (2011)), it is more likely that the ionizing flux comes from several stars. It possible that G25.4NW is powered by serveral O/B stars, with at least one earlier than an O7 star.

4.3 Ionized Gas Mass

For optically thin emission, the emission measure (EM) is related to the surface brightness (I_ν) according to the following formula (Osterbrock 1989):

$$I_\nu = 2\nu^2 k T_{b\nu}/c^2 = j_\nu \int n_i n_e ds = j_\nu EM, \tag{3}$$

where j_ν is the free-free emissivity for H^+ (3.45×10^{-40} ergs cm^{-3}s^{-1}Hz^{-1}sr^{-1} at 1420 MHz and 7500 K; after Lang 1980), n_i is the ion density, and n_e is the electron density. For j_ν of a pure hydrogen nebula one can write

$$EM = 5.77 \times 10^2 T_{b\nu} (\frac{T_e}{7500\ K})^{0.35} (\frac{\nu}{1.42\ GHz})^{2.1}\ [\mathrm{cm}^{-6}\ \mathrm{pc}] \tag{4}$$

$$T_{b\nu} = \frac{c^2 S_\nu 10^{-26}}{2k\nu^2\Omega}[K] \tag{5}$$

where T_e is the electron temperature in the nebula, S_ν is the integratged flux density in Jy and Ω is the radio source solid angle in steradians. The UCHII region was not resolved in the VGPS map (resolution 1 arcmin), but it is resolved in the high resolution map observed with the VLA B configuration (Giveon et al. 2005), from which we estimated that the souce has a size of 10.1″, corresponding to a physical size of ∼0.28 pc. Hence we derive $EM = 5.5\times10^6$ cm^{-6} pc using a typical value T_e = 10000 K. The electron density in the HII region can be calculated from the emission measures using the following formula (Giveon et al. 2007)

$$n_e = 990 \sqrt{(\frac{EM}{10^6 pc\ cm^{-6}})(\frac{pc}{D})}[cm^{-3}] \tag{6}$$

where D is the diameter of G25.4NW (∼ 0.28 pc). We find an average value of $n_e = 4.4 \times 10^3$ cm^{-3}. Assuming a spherical volume of ionized gas, we estimate G25.4NW contains 460 $M_\odot$ of ionized gas.

Comparing the EM and n_e values with those in Giveon et al. (2007) (after correcting the distance from 9.6 kpc to 5.7 kpc), our derived values are slightly lower than theirs. This is because we used a larger source size. Giveon et al. (2005) used the 5GHz VLA data to estimate a source size of 3.7″, thus they obtained values for a more compact HII region. As the NIR map of Zhu et al. (2011) has shown that there are at least 3 stars in the G25.4NW region, the VLA map at 1.4GHZ could not resolved the individual HII region, thus we could overestimate the source size. Nevertherless, our estimated values of EM and n_e can be used as a lower limit.

4.4 The Giant Molecular cloud surrounding G25.4NW

Figure 5 shows the ^{13}CO integrated (over the range 90-101 km s^{-1}) intensity contours overlaid on the IRAC 8μm image. The MIR 8μm emission is dominated by the PAH emissions that are heated by UV photons from young stars. The two bright regions in the map are the HII regions G25.4NW and W42. The W42 region is not physically related with G25.4NW. It is a foreground source at a different distance

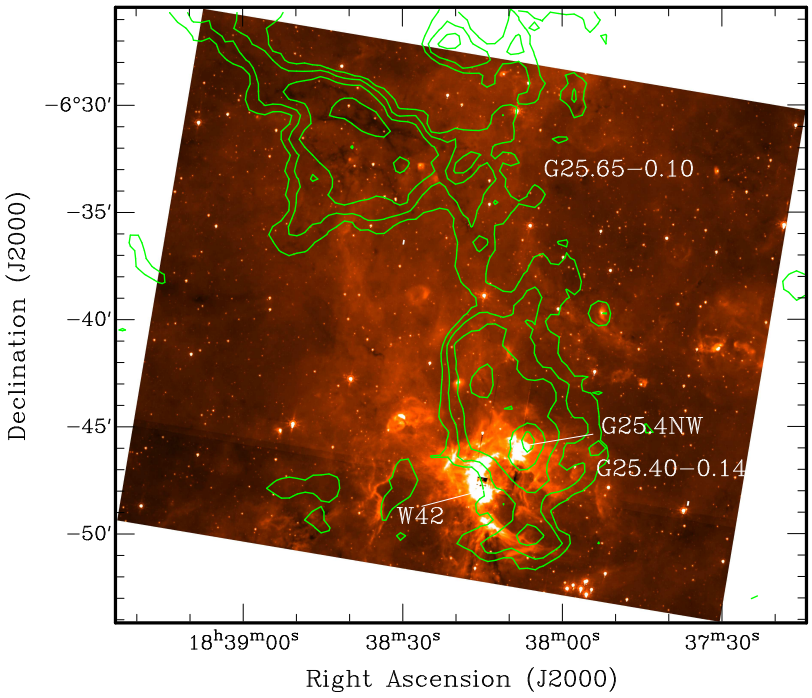

Fig. 5 The ^{13}CO integrated intensity contours overlaid on a Spitzer IRAC 8 μm image. The contours are plotted at 0.6 (3σ), 0.8, 1.1, 1.6, 2.2 K.

of 4.6 kpc (see Sect.3.2). We can see that G254.NW is embedded in a giant molecular complex, which appears to be divided into two major clouds: the fish-shape cloud G25.40-0.14 hosting G25.4NW and the other one G25.65-0.10 that peaks at (l=25.68 °, b=-0.13°). The later was named as G25.65-0.10 in the paper of Solomon et al. (1987), which appears to be associated with an IR dark cloud (IRDC). We note that Solomon et al. (1987) use G25.65-0.10 to refer to the GMC cloud at 94 km/s, with the size of 13′ × 8′, which did not include the G25.4-0.14 cloud. However, in our maps these two clouds appear to be associated with each other connected with low level contours (as shown in the 3σ contour), indicating a possible physical connection between G25.4-0.14 and G25.65-0.10 and they might belong to one GMC at the same distance. If confirmed, such a GMC would have a maximum physical size of about 36 pc (22′) at a distance of 5.7 kpc. The two separated major clouds and the existance of a number of local peaks in each cloud suggest that fragmentation is taking place in this complex, with G25.4NW being the most active region forming a cluster of massive stars. JCMT18354-0649S as another massive core that hosts a massive protostar is offset from the G25.4NW radio continuum by 1′, indicating that OB stars run away from their natal clouds and the HII region is more evolved. It appears that the formed massive stars is triggerring new star formation in JCMT18354-0649S. We have searched the literature and the SIMBA database, and there are no IR or radio sources associated with G25.65-0.10, suggesting that this cloud is relatively quiet and no star formation activity is taking place.

The total H_2 mass of the fish-shape CO cloud G25.4-0.14 (size: $12' \times 6'$) at 95±10 km s^{-1} is estimated using $M_{H_2} = N_{H_2}\Omega d^2(2m_H/M_\odot)$, where Ω is the solid angle of the cloud, and d is its distance of 5.7 kpc. Assuming the CO cloud is under thermodynamic equilibrium (LTE) and the ^{13}CO is optically thin and using the fitted dust temperature of 42.5 K, we obtained a ^{13}CO column density of the cloud is $N_{^{13}CO} = 2.91 \times 10^{17}$ cm^{-2} from the ^{13}CO integrated map (over the range 90-101 km s^{-1}). Then we obtain an average H_2 column density of $N_{H_2} = 4.59 \times 10^5 N_{^{13}CO} \approx 1.33 \times 10^{23}$ cm^{-2}, and a molecular cloud mass of $M_{H_2} \approx 1.0 \times 10^4$ $M_\odot$. This molecular cloud has a mean density of $\sim 2.3 \times 10^4$ cm^{-3}.

5 SUMMARY

In Summary, using new VLA continuum and HI-line data for G25.4NW, we have obtained HI absorption profiles towards the UCHII region. G25.4NW shows HI absorption features up to 95 km s^{-1}, and there is not any other absorptions up to the tangential velocity, giving a near-side distance of 5.7 kpc. The detected HI absorption and CO emission is coincident with the expected velocity for a galactic molecular ring region at 4-6 kpc from the Galactic arms model. Using the new distance, we obtain a bolometric luminosity of $10^{5.6}$ $L_\odot$ from collected IR emission from G25.4NW, which correspond to an O6 star. We also use the radio continuum emission data confirm this results, and re-calculate the EM and electronic density n_e. We estimated that G25.4NW contains 460 $M_\odot$ of ionized gas. The ^{13}CO data reveal that G25.4NW is part of a more extended star-formation complex with about 10^4 $M_\odot$ molecular gas.

Acknowledgements We acknowledges the supports from NSFC grant 11073028 and also from the "Hundred-talent program" of Chinese Academy of Sciences. We thanks Prof. Wenwu Tian, Yuefang Wu and Dr. Lei Zhu for reviewing the manuscript and providing helpful instruction. We thank the anonymous referee for his instructive and useful comments.

References

Anderson, L. D., & Bania, T. M. 2009, ApJ, 690, 706
Benjamin, R. A., Churchwell, E., Babler, B. L., et al. 2003, PASP, 115, 953
Blum, R. D., Conti, P. S., & Damineli, A. 2000, AJ, 119, 1860
Carolan, P. B., Khanzadyan, T., Redman, M. P., et al. 2009, MNRAS, 400, 78
Churchwell, E., Walmsley, C. M., & Cesaroni, R. 1990, A&AS, 83, 119
Cordes, J. M., & Lazio, T. J. W. 2002, arXiv:astro-ph/0207156
Downes, D., Wilson, T. L., Bieging, J., & Wink, J. 1980, A&AS, 40, 379
Fazio, G. G., Hora, J. L., Allen, L. E., et al. 2004, ApJS, 154, 10
Fich, M., Blitz, L., & Stark, A. A. 1989, ApJ, 342, 272
Giveon, U., Becker, R. H., Helfand, D. J., & White, R. L. 2005, AJ, 129, 348
Giveon, U., Richter, M. J., Becker, R. H., & White, R. L. 2007, AJ, 133, 639
Jackson, J. M., Rathborne, J. M., Shah, R. Y., et al. 2006, ApJS, 163, 145
Lester, D. F., Dinerstein, H. L., Werner, M. W., et al. 1985, ApJ, 296, 565
Liu, T., Wu, Y., Zhang, Q., et al. 2011, ApJ, 728, 91
Osterbrock, D. E. 1989, S&T, 78, 491
Panagia, N. 1973, AJ, 78, 929
Rudolph, A. L., Brand, J., de Geus, E. J., & Wouterloot, J. G. A. 1996, ApJ, 458, 653
Solomon, P. M., Rivolo, A. R., Barrett, J., & Yahil, A. 1987, ApJ, 319, 730
Stil, J. M., Taylor, A. R., Dickey, J. M., et al. 2006, AJ, 132, 1158
Tian, W. W., & Leahy, D. A. 2008, ApJ, 677, 292
Tian, W. W., Leahy, D. A., & Li, D. 2010, MNRAS, 404, L1
Turner, B. E. 1979, A&AS, 37, 1
Wu, Y., Zhu, M., Wei, Y., et al. 2005, ApJ, 628, L57
Zhu, M., Davis, C. J., Wu, Y. F., et al. 2011, ApJ, 37, 1